Lysosome-mediated degradation of a distinct pool of lipid droplets during hepatic stellate cell activation

Received for publication, January 26, 2017, and in revised form, June 14, 2017 Published, Papers in Press, June 14, 2017, DOI 10.1074/jbc.M117.778472

Maidina Tuohetahuntila[‡], Martijn R. Molenaar[‡], Bart Spee[§], Jos F. Brouwers[‡], Richard Wubbolts[‡], Martin Houweling[‡], Cong Yan[¶], Hong Du[¶], Brian C. VanderVen[‖], Arie B. Vaandrager[‡], and J. Bernd Helms[‡1]

From the [‡]Department of Biochemistry and Cell Biology, Faculty of Veterinary Medicine, Utrecht University, 3584 CM, Utrecht, The Netherlands, [§]Department of Clinical Sciences of Companion Animals, Faculty of Veterinary Medicine, Utrecht University, 3584 CM, Utrecht, The Netherlands, [¶]Indiana University School of Medicine, Indianapolis, Indiana 46202, and [‖]Department of Microbiology and Immunology, Cornell University, C5 181 Veterinary Medicine Center, Ithaca, New York 14853

Edited by George M. Carman

Activation of hepatic stellate cells (HSCs) is a critical step in the development of liver fibrosis. During activation, HSCs lose their lipid droplets (LDs) containing triacylglycerols (TAGs), cholesteryl esters, and retinyl esters (REs). We previously provided evidence for the presence of two distinct LD pools, a preexisting and a dynamic LD pool. Here we investigate the mechanisms of neutral lipid metabolism in the preexisting LD pool. To investigate the involvement of lysosomal degradation of neutral lipids, we studied the effect of lalistat, a specific lysosomal acid lipase (LAL/Lipa) inhibitor on LD degradation in HSCs during activation *in vitro*. The LAL inhibitor increased the levels of TAG, cholesteryl ester, and RE in both rat and mouse HSCs. Lalistat was less potent in inhibiting the degradation of newly synthesized TAG species as compared with a more general lipase inhibitor orlistat. Lalistat also induced the presence of RE-containing LDs in an acidic compartment. However, targeted deletion of the Lipa gene in mice decreased the liver levels of RE, most likely as the result of a gradual disappearance of HSCs in livers of Lipa$^{-/-}$ mice. Lalistat partially inhibited the induction of activation marker α-smooth muscle actin (α-SMA) in rat and mouse HSCs. Our data suggest that LAL/Lipa is involved in the degradation of a specific preexisting pool of LDs and that inhibition of this pathway attenuates HSC activation.

The majority of vitamin A (retinol) is stored as retinyl esters (REs)[2] in specific liver cells, the so-called hepatic stellate cells (HSCs) (1, 2). HSCs are located in the spaces of Disse, between sinusoidal endothelial cells and hepatocytes. In a healthy liver, HSCs contain large lipid droplets filled with REs, triacylglycerols (TAGs), and cholesteryl esters (CEs). After liver injury, quiescent HSCs can transdifferentiate into activated cells with a myofibroblastic phenotype (1). Activated macrophages in concert with HSCs may initiate this transition by secreting cytokines such as transforming growth factor β (TGF-β), which stimulate the synthesis of matrix proteins and the release of retinoids by HSCs (1, 3). The loss of retinoids is associated with a gradual disappearance of LDs in HSCs. We previously reported that LD degradation in activated rat HSCs occurs in two phases (4). Upon activation of HSCs, the LDs reduce in size but increase in number during the first 7 days in culture. In the second phase the lipid droplets disappear. Raman and lipidomic studies showed that in the initial phase of HSC activation, the REs disappear rapidly, whereas the TAG content transiently increases (4). This increase in TAGs in rat HSCs is predominantly caused by a large and specific increase in polyunsaturated fatty acid (PUFA)-containing triacylglycerol species during the first 7 days in culture, mediated by the increase in the ratio of the PUFA-specific fatty acid CoA synthase 4 (ACSL4) to the nonspecific ASCLs, especially ASCL1 (5).

The observed increase in the number of LDs during the first phase of HSC activation can in principle be accomplished by the *de novo* synthesis of the new LDs (6) or fission of existing large LDs (7). We previously suggested that HSCs contain two pools of LDs, a preexisting and a dynamic pool of LDs. The preexisting LD pool is characterized by a larger average size of the LD diameter, the presence of REs, and the involvement of its synthesizing enzyme LRAT (8, 9). The dynamic LDs were shown to be smaller than preexisting LDs and have a dynamic lipid metabolism, with new TAG synthesis and hydrolysis at relatively high rates (9). We previously demonstrated that the observed increase in number of LDs during the first phase of HSC activation is likely the result of a decrease of the preexisting pool of LDs and concomitant presence of a highly dynamic pool of lipid droplets. In the dynamic LD pool, DGAT1 and ATGL (also known as PNPLA2) are involved in the synthesis and breakdown of newly synthesized TAGs, respectively (9). The degradation pathway of the dynamic LD pool resembles the well known mechanism of LD breakdown in adipose cells. In these cells key roles were assigned to ATGL, its co-activator

This work was supported by the seventh framework program of the EU-funded "LipidomicNet" project (proposal number 202272). The authors declare that they have no conflicts of interest with the contents of this article.

This article contains supplemental Tables S1 and S2 and Figs. S1–S3.

[1] To whom correspondence should be addressed: Dept. of Biochemistry and Cell Biology, Utrecht University, Faculty of Veterinary Medicine, Yalelaan 2, 3584 CM Utrecht, The Netherlands. Tel.: 31-30-2535375; Fax: 31-30-2535492; E-mail: J.B.Helms@uu.nl.

[2] The abbreviations used are: RE, retinyl ester; HSC, hepatic stellate cell; ACSL, long chain fatty acid CoA synthase; ATGL, adipose triglyceride lipase; CE, cholesteryl ester; DGAT, acyl-CoA:diacylglycerol acyltransferase; FA, fatty acid; LAL, lysosomal acid lipase; LD, lipid droplet; Lipa, lysosomal acidic lipase gene; LRAT, lecithin:retinol acyltransferase; PUFA, polyunsaturated fatty acid; qPCR, quantitative PCR; REH, retinyl ester hydrolase; SMA, smooth muscle actin; TAG, triacylglycerol; RP, retinyl palmitate; PF, paraformaldehyde; MRM, multiple reaction monitoring; D7-CE, D7-cholesteryl palmitate.

CGI-58, and hormone-sensitive lipase (10). The first two proteins are known to have a more general function as deficiencies in either one leads to neutral lipid storage diseases (11). Rat HSCs were shown to express ATGL but not hormone-sensitive lipase (9, 12).

In mouse and rat HSCs, ATGL was found to be involved specifically in breakdown of newly synthesized TAGs but not in degrading TAGs in the preexisting LD pool. This suggests the existence of another lipolysis pathway (9). In mouse HSCs, lipid breakdown was shown to be partially mediated by a lipophagic pathway, as inhibition of autophagy increased the amount of LDs (13–15). Because inhibition of autophagy was shown to impair HSC activation in mice and this effect could be partially reversed by the addition of exogenous FAs, it was suggested that LD breakdown is required to fulfill the energy demands of HSCs during activation (14).

The lipase active in lipophagy is thought to be lysosomal acid lipase (LAL), which is encoded by the Lipa gene (16) and which is also responsible for the degradation of lipoprotein derived CEs and TAGs taken up by endocytosis (17). Targeted deletion of Lipa in mice leads to severe CE and TAG accumulation in hepatocytes (18), and LAL deficiency in humans results in either Wolman disease or its milder variant, cholesteryl ester storage disease (CESD), depending on the mutation in the Lipa gene (19).

In this study we addressed the question of whether inhibition of LAL affects lipid metabolism in HSCs and the activation process in rat and mouse HSCs. We, therefore, studied the effect of the LAL-specific inhibitor lalistat (20–22) on HSC lipid metabolism and activation, and we made use of a knockout strain of mice deficient in LAL.

Results

Neutral lipid breakdown in HSCs by lysosomal acidic lipase

The contribution of LAL/Lipa to neutral lipid breakdown was studied by incubating rat HSCs with the LAL-specific inhibitor lalistat (100 μM) during the early activating phase (days 1–7). As shown in Fig. 1*A*, lalistat caused a 3–4-fold increase in the levels of all neutral lipids including TAGs, CEs, and REs. Lalistat (100 μM) proved to be non-toxic to the HSCs, as the 6-day incubation had no effect on cell viability (98 $\pm$ 13% of control viable cells). The increase in TAGs and CEs could be (partially) the result of uptake of exogenous lipids, *e.g.* as lipoproteins, from the medium that are also degraded by LAL. To determine whether the observed increase in neutral lipids during HSC activation by lalistat resulted from inhibition of breakdown of extracellular or intracellular neutral lipids, we limited the contribution of exogenous lipids during the inhibitor treatment by culturing the cells in medium with delipidated serum. Under these conditions the levels of TAG species containing PUFAs and the levels of CEs were much lower (Fig. 1*B*), in line with the notion that PUFA-TAGs are synthesized from exogenous PUFAs (5) and that CEs are derived from lipoproteins from the medium. The levels of non-PUFA TAGs were less affected by growing the HSCs in delipidated medium. Nevertheless, the levels of these non-PUFA TAGs and REs were increased by lalistat to similar levels when compared with cells grown in normal medium (*cf.* Fig. 1, *A* and *B*). During the incubation with delipidated medium, TAGs might still be (re)synthesized from endogenous FAs, derived from TAG and phospholipid breakdown. We, therefore, also studied the effect of lalistat in delipidated medium and in the presence of T863, a DGAT1 inhibitor that was shown to inhibit TAG synthesis in rat HSCs for >80% (9). When re-synthesis is inhibited, the amount of non-PUFA TAGs is almost halved during the 3-day incubation, similar to the ~60% decrease in RE levels (Fig. 1*C*). Lalistat completely prevented the degradation of these lipids, clearly indicating that this LAL inhibitor prevented the breakdown of preexisting lipids. To determine the specificity of lalistat, we tested the pyrazole-methanone compounds E4, F2, and H4, which have been described to inhibit LAL (23). As shown in Fig. 1*D*, the potency of the compounds to increase the level of CEs, a clear hallmark of LAL-inhibition (18), was correlated to their capacity to increase the levels of TAGs and REs. The lalistat-induced accumulation of non-PUFA TAGs and REs is opposite from our previous observation that HSCs from ATGL-deficient mice accumulated PUFA-TAGs but not non-PUFA TAGs and REs (9). As ATGL is involved in the turnover of lipids in the dynamic LD pool (9), our combined results indicate that Lalistat does not affect the dynamic LD pool but, rather, the preexisting LD pool.

The dynamic LD pool can be readily labeled by the addition of deuterated fatty acids to the medium resulting in rapid incorporation of the stable isotope in this pool of lipids (9). To investigate directly whether the LAL inhibitor could inhibit the dynamic TAG pool, we labeled freshly isolated rat HSCs for 2 days with 25 μM D4-palmitate in medium containing 10% fetal bovine serum followed by a 2-day chase without stable isotope-labeled palmitate but in the presence of lalistat or orlistat, a general lipase inhibitor formerly known as tetrahydrolipstatin (20, 24). As shown in Fig. 2*A*, a large percentage of TAGs can be labeled with D4-palmitate. In the absence of inhibitors, the doubly labeled TAG species are almost completely degraded during the 2-day chase (Fig. 2, *A* and *B*). The general lipase inhibitor orlistat could inhibit the degradation of the newly made TAGs almost completely. However, lalistat did not significantly affect the degradation of the labeled TAGs. Both lalistat and orlistat increased the amount of unlabeled TAGs during the chase to a similar level (Fig. 2). This suggests that lalistat preferentially inhibits the degradation of a pool of unlabeled TAGs, whereas orlistat affects the breakdown of both a pool of labeled (*i.e.* newly synthesized) and unlabeled (preexisting) TAGs.

Lalistat affected LD morphology and localization

The observed lalistat-induced increase of a specific pool of neutral lipids might lead to changes in LD size and/or number. Examination of lipid droplet morphology in HSCs by fluorescence microscopy showed that lalistat induces an increase in the number, but not in the size of the of LDs, whereas orlistat increased both parameters, resulting in a specific increase in big LDs (>2 μm) (Fig. 3). These data are in agreement with the fact that these drugs affect different lipid breakdown pathways. To verify that lalistat inhibits lipid breakdown in the lysosomal compartment, we imaged LDs in HSCs after

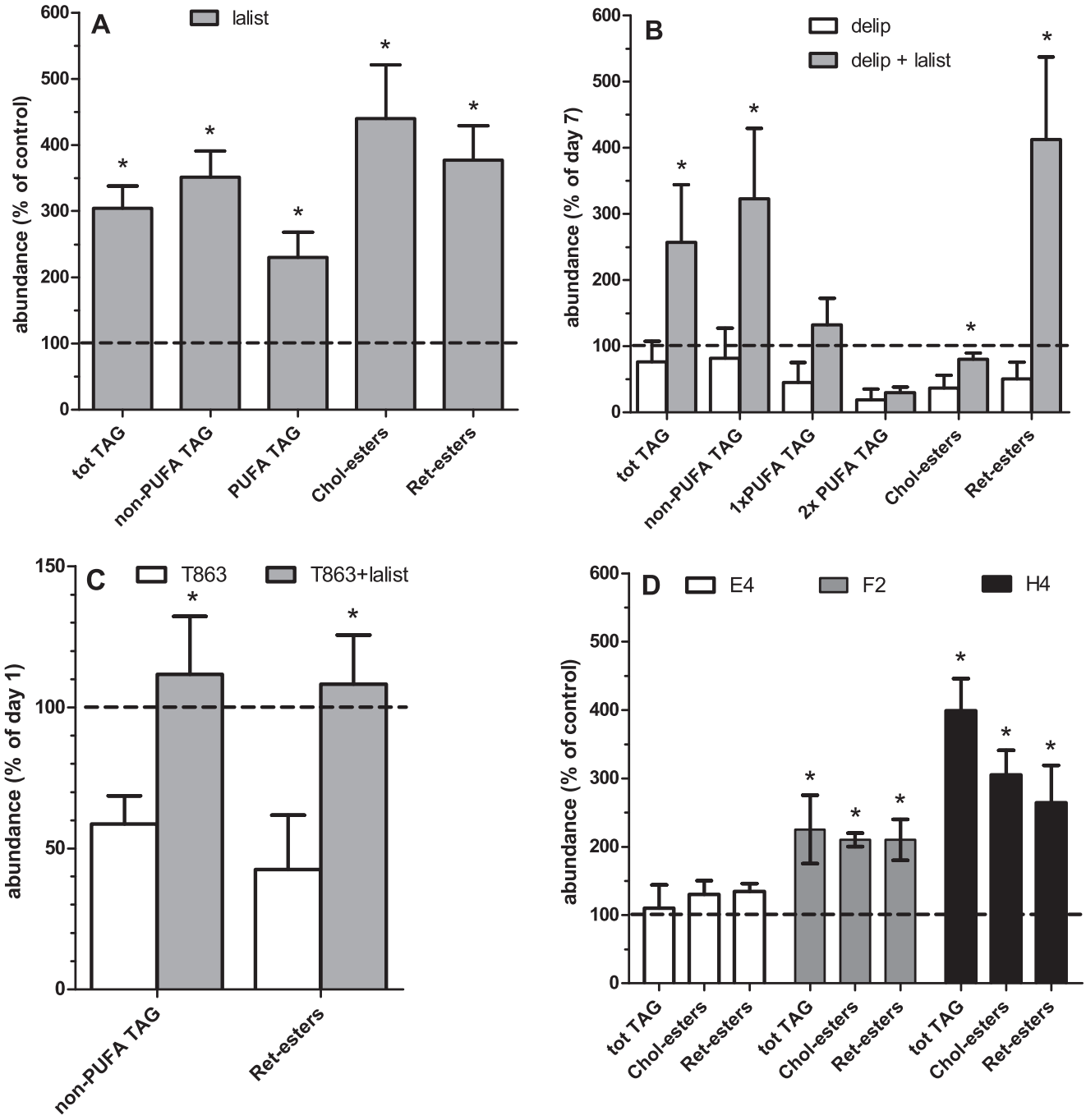

Figure 1. The lysosomal lipase inhibitor lalistat increased the levels of neutral lipids in rat HSCs. *A* and *B*, isolated rat HSCs were incubated from day 1 to day 7 in medium with 10% FBS (*A*) or 10% delipidated FBS (*delip*) (*B*) containing vehicle (DMSO) or 100 μM lalistat (*lalist*). *C*, isolated rat HSCs were incubated from day 1 to day 4 in medium with delipidated FBS and 10 μM DGAT1 inhibitor T863 additionally containing vehicle (DMSO; *T863*; *white bars*) or 100 μM lalistat (*T863*+*lalist*; *gray bars*). *D*, isolated rat HSCs were incubated from day 1 to day 7 in medium with 10% FBS containing vehicle (DMSO) or 10 μM pyrazole-methanone compounds E4, F2, or H4. Subsequently, neutral lipids were determined by HPLC-MS. The values were normalized to the amount of cholesterol in the sample and expressed relative to the level of the respective lipids present in the control cells incubated with FBS at day 7 (*A*, *B*, and *D*) or to the level of the respective lipids present in the cells at day 1 (*C*). Data are the means ± S.E. of 6 experiments performed in duplicate (*A*) or the means ± S.D. of 3 (*B* and *D*) or 4 (*C*) experiments performed in duplicate. *, $p < 0.05$, *t* test *versus* control.

staining the acidic compartments with Lysotracker red (Fig. 4). In control cells we observed that ~20% of the Lysotracker positive structures were close to RE-containing LDs, but colocalization was not observed. Only in the HSCs incubated with lalistat did we detect a consistent colocalization of these structures, indicating that the lipids accumulated inside lysosomes (Fig. 4 and supplemental Fig. S1). After incubation with lalistat we also noticed HSCs that clearly contained two populations of LDs, one that contained retinoids (UV autofluorescent), and one that did not (Fig. 4*A* and supplemental Fig. S1). Typically, the latter population was localized at the periphery of the cell, whereas the former was present around the nucleus together with the Lysotracker red-positive structures.

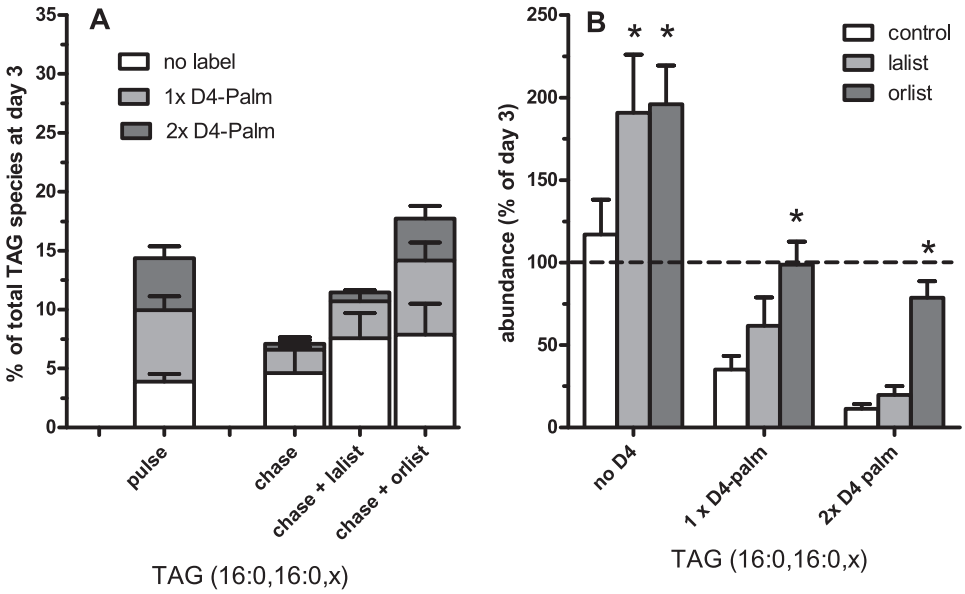

Figure 2. Lalistat did not affect the degradation on newly synthesized TAG species in rat HSCs. Primary rat HSCs were incubated on day 1 with 25 μM D4-palmitate for 48 h. At day 3, part of the cells were harvested (*pulse*), and the remaining HSCs were chased for 48 h with normal medium with vehicle (DMSO; *control*), 100 μM lalistat (*lalist*), or 40 μM orlistat (*orlist*) and harvested at day 5 (chase). *A*, single or double deuterium-labeled (*gray* and *dark gray bars*) and non-labeled (*white bars*) TAG fragments with two palmitoyl chains (16:0,16:0,*x*) were quantitated and expressed as the percentage of all TAG species. *B* shows breakdown of TAG species from *panel A*, as the levels of the indicated TAG fragments at day 5, after the chase, were expressed relative to the level of the same TAG species at the beginning of the chase at day 3. Data are the means ± S.D. of five experiments performed in duplicate. *, $p < 0.05$ paired *t* test *versus* control.

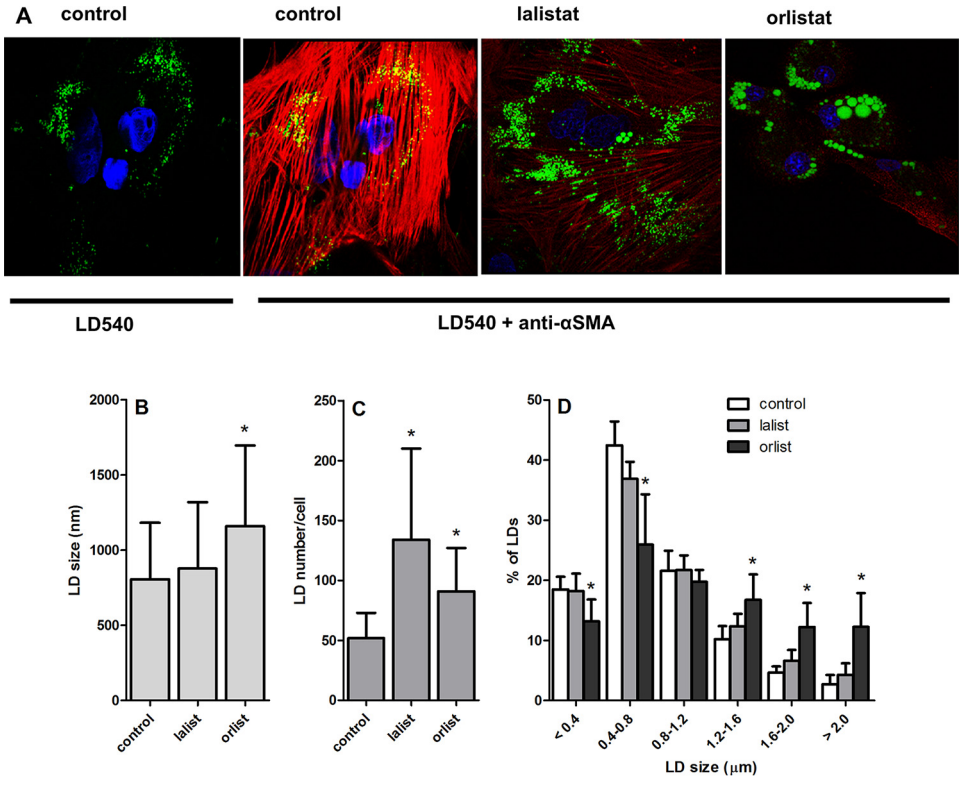

Figure 3. Effect of lalistat and orlistat on LD morphology and on the activation marker α-SMA in rat HSCs. *A*, confocal images of HSCs isolated from rats incubated from day 1 to day 7 with vehicle (day 7), 100 μM lalistat, or 40 μM orlistat. Lipid droplets were stained with LD540 dye (*green*) and anti α-SMA antibody (*red*), and nuclei were stained with Hoechst (*blue*). In the *first panel* the red channel was omitted for better visibility of the LDs. Shown are representative pictures from four experiments. *B–D*, images were analyzed with CellProfiler v2.1.1. *B*, LD size was expressed in diameter (nm). *C*, LD numbers were expressed as a ratio of scored lipid droplets and scored nuclei per image. *D*, LDs distribution is expressed as percentage of LDs with the specified size (in μm). Image analysis was based on at least 50 cells and 3000 lipid droplets per condition. Data are the means ± S.D. *, $p < 0.05$ *t* test *versus* control.

Retinyl ester breakdown in HSCs by lysosomal acidic lipase

The observed inhibitory effect of lalistat on RE degradation and accumulation of REs in lysosomes suggests that the Lipa gene product has RE hydrolytic (REH) activity. Previously, an acidic REH has been described that was different from LAL/Lipa as judged from its insensitivity to bivalent metal ions like

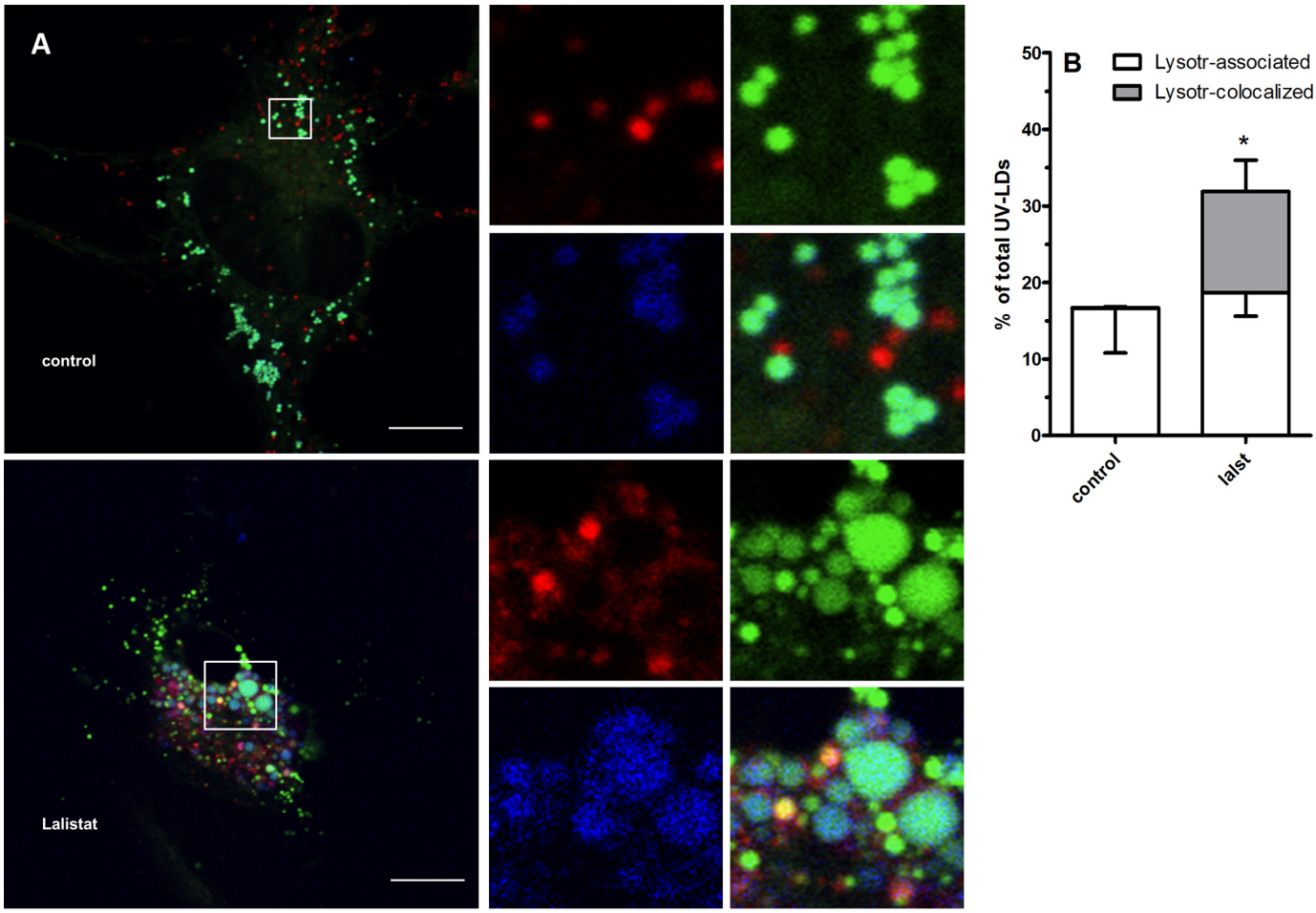

Figure 4. Lalistat increased colocalization of LD and the lysosomal compartment in rat HSCs. *A*, confocal images of HSCs isolated from rats incubated from day 1 to day 4 in medium with 10% FBS in the presence of vehicle (*control*) or 100 μM lalistat. Live HSCs were stained with Lysotracker Red DND99 (*red*) and Bodipy (LD dye, *green*) for 30 min before imaging. *Blue* is the UV autofluorescence signal from REs. In the *boxes* higher magnification of the separate channels and the merge are shown. The *white bar* is 10 μm. *B*, UV-positive LDs were counted and classified manually. Classifications were (i) not in contact with Lysotracker red structures, (ii) in contact or surrounded by Lysotracker red structures (*Lysotr.-associated*; *white bars*) or completely colocalized with Lysotracker red structures (*Lysotr.-colocalized*; *gray bars*). Image analysis was based on 40 cells from 4 independent experiments. Data are the means ± S.E. *, $p < 0.05$, *t* test *versus* control.

Ca^{2+} and Mg^{2+} (25, 26). We also found that the main REH in a homogenate of rat HSCs and rat hepatocytes has an optimum at pH 4 (Fig. 5, *A* and *B*). However, we could not observe a difference in inhibition by bivalent cations between the REH in comparison to the CE hydrolase activity, assayed simultaneously (Fig. 5*B*). We also found that both activities were inhibited by lalistat (Fig. 5*B*), with a similar IC_{50} ~1–3 μM. Furthermore, the acidic REH activity was absent in liver homogenates from $Lipa^{-/-}$ mice and could be induced in CHO homogenates by transfecting the CHO cells with recombinant rat Lipa (Fig. 5, *C* and *D*). These latter experiments clearly show that Lipa has REH activity *in vitro*.

To investigate the effect of Lipa on RE metabolism in HSCs, we attempted to isolate HSCs from $Lipa^{-/-}$ mice. However, isolation of $Lipa^{-/-}$ HSCs was not possible, most likely due to the massive accumulation of lipids in the $Lipa^{-/-}$ livers (18). Therefore, we analyzed the RE content in livers of Lipa-deficient and corresponding WT mice. Surprisingly, we found that despite the 100-fold higher levels of CEs (Fig. 6*A*), the levels of the REs were similar (retinyl stearate) or lower (retinyl palmitate and retinyl oleate) in the livers of 7-week-old $Lipa^{-/-}$ mice (Fig. 6*B*). In older mice (4–5 months; average 20 weeks), the difference between the WT and the Lipa-deficient mice became even larger, as the WT mice continued to accumulate REs, and the $Lipa^{-/-}$ mice lost most of their REs (Fig. 6*B*). The low levels of REs in the livers of the 4–5-month-old $Lipa^{-/-}$ mice were accompanied by a decrease in the expression of LRAT mRNA, considered a marker for quiescent HSCs (27), but not by an up-regulation of the HSC activation marker α-smooth muscle actin (α-*SMA*; Fig. 6, *C* and *D*). This suggests that the livers of the $Lipa^{-/-}$ mice gradually lose their HSCs.

To exclude that the apparent discrepancy between the lack of effect of Lipa knock out in mice *in vivo* on RE storage and the observed effect of the Lipa-inhibitor lalistat on RE levels in rat HSCs *in vitro* is caused by species differences between rat and mouse, we compared the effect of lalistat on neutral lipid levels in primary mouse HSCs with its effect on rat HSCs (*cf.* Figs. 7 and 1*A*). The levels of REs in primary isolated mouse HSCs at day 1 (5.5 ± 3 nmol of RE/mg of protein) were found to be similar to that in rat HSCs (6 ± 4 nmol of RE/mg of protein). We found that lalistat also caused an increase in TAGs, CEs, and REs in mouse HSCs. In comparison to rat HSCs, the lal-

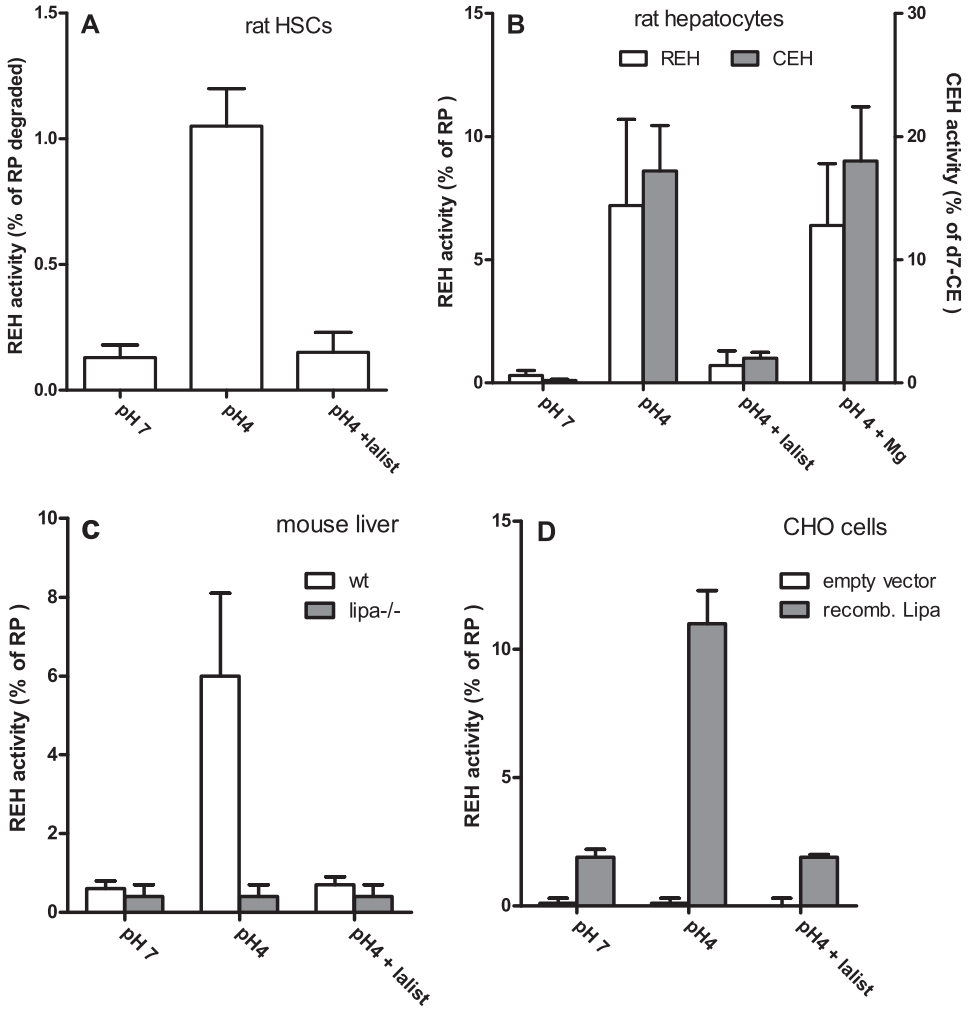

Figure 5. LAL/Lipa had retinyl esterase activity *in vitro*. REH was assayed with RP presented in liposomes as substrate in a buffer with pH 7, pH 4, and pH 4 containing 10 μM lalistat or pH4 containing 10 mm $MgCl_2$ in homogenates of primary rat HSCs cultured for 4 days (16 μg of protein) (*A*), freshly isolated rat hepatocytes (400 μg of protein) (*B*), whole mouse livers (400 μg of protein) (*C*), or cultured CHO cells 1 day after transfection with an empty expression vector or with an expression vector containing rat Lipa cDNA (40 μg of protein) (*D*). In *B*, cholesterol esterase activity (*CEH*) was assayed with D7-cholesterol oleate as substrate presented in liposomes together with RP. Free retinol, RP, D7-cholesterol, and D7-CE levels were quantitated by HPLC-MS in the MRM mode. Retinol and D7-cholesterol are expressed relative to the levels of their respective esters present at the start of the incubation. Data are the means ± S.D. of three experiments performed in duplicate.

istat-induced increase in RE level in mouse was somewhat lower (2.5-fold *versus* almost 4-fold in rat HSCs).

Rat HSCs have an active autophagy pathway that is required for cell survival

Determination of Lipa mRNA expression in quiescent (day 1) and activated (day 7) rat HSCs shows that Lipa mRNA is up-regulated during activation *in vitro* (Fig. 8*A*). Endogenous neutral lipids are thought to traffic to the lysosomal compartment by the autophagy pathway. An active autophagy pathway has indeed been described in activated mouse HSCs (13–15). To investigate the involvement of the autophagy pathway in rat HSCs, we made use of the autophagy marker protein LC3B, which can be detected as two isoforms; one represents the cytosolic LC3B-I and the other one represents LC3B-II, which is conjugated with phosphatidylethanolamine and is present on autophagosomes. The amount of LC3B-II is closely related to the autophagosome number and is a good indicator for activation of the autophagy pathway (28). Primary rat HSCs have a high ratio of the lipidated to unlipidated form of the autophagy protein LC3B already at day 1 and which continues until day 7 (Fig. 8*B*). As a control, the presence of LC3B-I and LC3B-II in LX-2 cells is shown. LX-2 cells are the human HSC cell line with a mixed phenotype with characteristics that resemble both the quiescent and activated phenotype (29). LX-2 cells have a low lipidated to unlipidated ratio that changes upon stimulation of the autophagy pathway (Fig. 8*B*). Autophagy was also detected in rat HSCs by Cyto-ID® staining (supplemental Fig. S2). Cyto-ID-positive structures and lipid droplets are abundantly present in HSCs at day 3, but only in the presence of lalistat colocalization of these structures is observed.

To study the contribution of the autophagy pathway in LD breakdown, we attempted to inhibit this pathway with specific inhibitors including 3-methyladenine (5 mM) and bafilomycin A1 (7.5 nM) and with the inhibitor of lysosomal degradation chloroquine (5 μM). All these inhibitors caused massive death of the rat HSCs within 12 h, although the doses used did not affect the viability of the human stellate cell line LX-2 (results

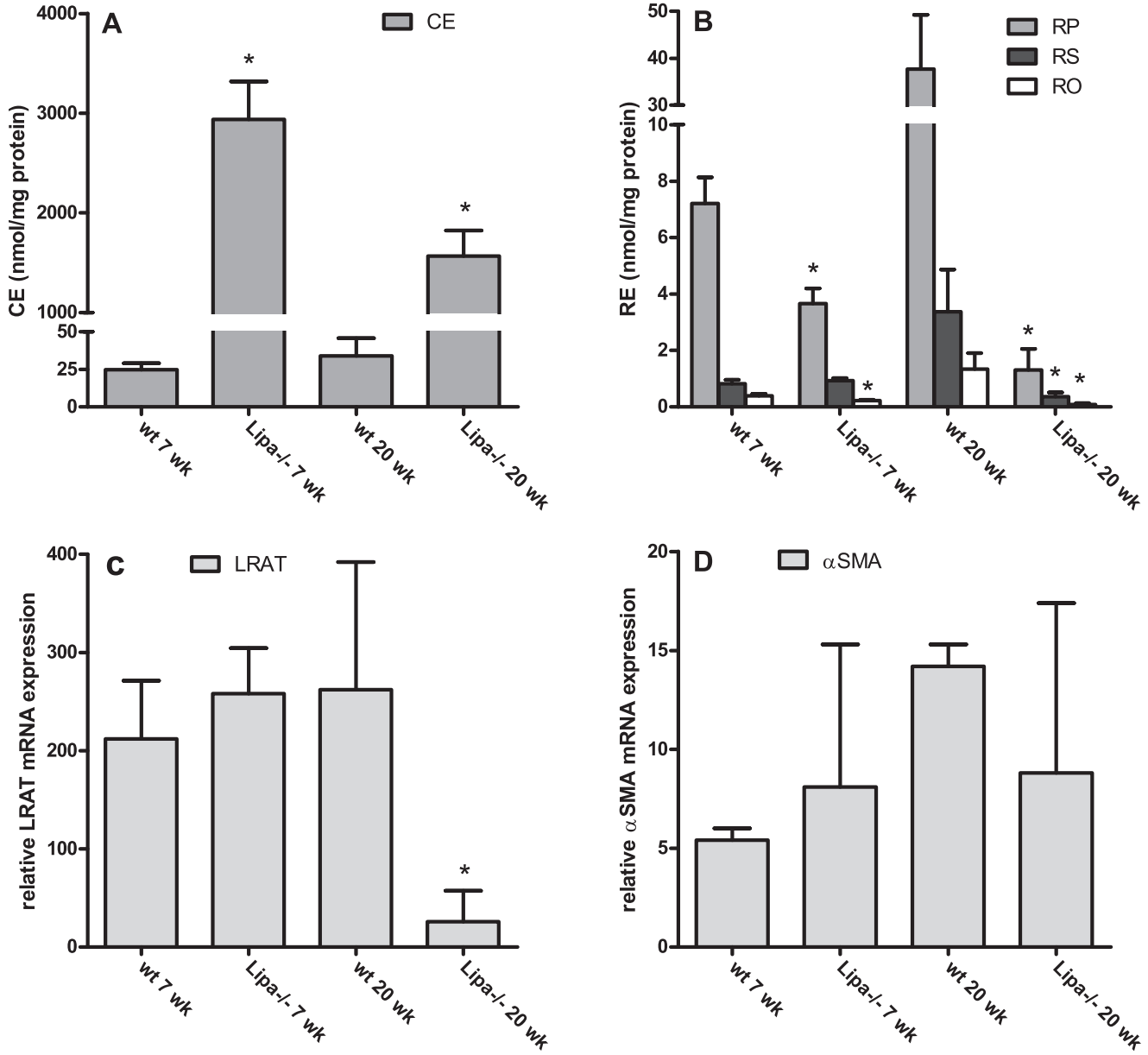

Figure 6. Retinyl esters did not accumulate in livers of LAL-deficient mice. Livers were obtained from either WT and Lipa$^{-/-}$ mice at an age of 7 weeks (*wk*) or between 4 and 5 months (20 weeks). *A* and *B*, CEs (*panel A*) and REs (*panel B*) were quantitated by HPLC-MS in the MRM mode. The following REs were analyzed: RP (*gray bars*), retinyl stearate (*RS*; *dark gray bars*), and retinyl oleate (*RO*; *white bars*). *C* and *D*, the relative mRNA expression of LRAT (a marker for quiescent HSCs; *panel C*) and α-SMA (HSC activation marker; *panel D*) was measured by qPCR. Data are the means ± S.D. of 5 mice (20 weeks) or 4 mice (7 weeks), assayed in duplicate. *, $p < 0.05$ *t* test *versus* WT.

not shown). When we studied the autophagy inhibitors in rat HSCs at lower concentrations that were tolerated, we could not find an effect of these inhibitors on autophagy or lysosomal acidification as analyzed with the LC3B-I to -II ratio and imaging with Lysotracker red (results not shown). From these data we conclude that rat HSCs in culture have a very active autophagy pathway, already as early as day 1 after isolation. The ratio of lipidated to unlipidated LC3B is markedly lower in mouse HSCs (13, 14), and this may explain the high sensitivity of rat HSCs toward autophagy inhibitors, as autophagy seems more essential for rat HSCs as compared with mouse HSCs, at least under our culture conditions.

We considered the possibility that the essential role of autophagy in rat HSCs is the result of an essential reutilization of nutrients from the autophagy pathway. A highly active autophagy pathway in rat HSCs may, therefore, suggest an active turnover of the preexisting LD pool. To study this in more detail, we took advantage of the RE metabolism in HSCs. We previously showed that retinol is generated from hydrolysis of endogenous REs and is available for re-synthesis of REs in either the preexisting (LRAT-mediated) or dynamic pool (DGAT1-mediated) of LDs (8). Indeed, after the addition of deuterated fatty acids to the cell culture medium, we not only observed an incorporation of D4-labeled palmitate into TAGs (Fig. 2) but also a significant D4-labeling of retinyl palmitate (RP) (~30%) (Fig. 8*C*). This indicates that a significant part of the retinyl palmitate is re-synthesized from endogenous retinol, derived from the breakdown of endogenous REs, as the medium

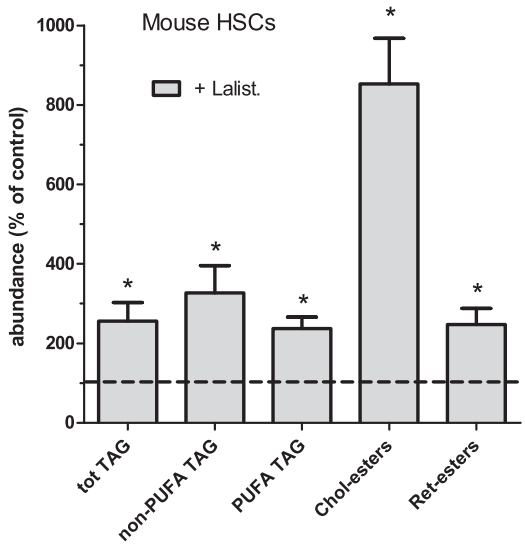

Figure 7. Effect of lalistat on neutral lipid levels in mouse HSCs. Isolated mouse HSCs were incubated from day 1 to day 7 in medium with 10% FBS containing vehicle (DMSO; control) and 100 μM lalistat (*Lalist*). Subsequently, neutral lipids were determined by HPLC-MS. The values were normalized to the amount of cholesterol in the sample and expressed relative to the level of the respective lipids present in the control cells at day 7. Data are the means ± S.E. of six experiments performed in duplicate. *, $p < 0.05$ *t* test *versus* control.

contained almost no retinol nor REs (results not shown). In line with this, we found that lalistat, which was shown to inhibit the breakdown of the existing REs (Fig. 1) and thus expected to prevent the release of free retinol, clearly prevented the incorporation of D4-palmitate into REs (Fig. 8*C*).

The RE species distribution changes during HSC activation. In quiescent HSCs, retinyl palmitate is the predominant RE species (>80%) in preexisting LDs (8). Upon activation, the percentage of retinyl palmitate species drops, reflecting RE synthesis by DGAT1 in the dynamic LD pool. If lalistat inhibits the breakdown of REs from the preexisting LD pool, then it is expected that lalistat also prevents the remodeling of the RE pool during activation as reflected in the change in retinyl ester species distribution (8). Indeed, at day 1 the predominantly retinyl ester is palmitate (84 ± 3%) in rat HSCs, whereas after activation on day 7 a more diverse species distribution was observed (Fig. 8*D*). In the presence of lalistat, the species distribution at day 7 more resembled that on day 1 with 74 ± 4% retinyl palmitate.

Lalistat inhibited HSC activation

To investigate whether the change in neutral lipid metabolism by the LAL inhibitors or orlistat has an effect on the activation process, we determined the expression levels of α-SMA. α-SMA is considered a marker for HSC activation and was clearly up-regulated in mouse and rat HSCs at day 7 (9). We observed a clear inhibition of the expression of α-SMA by both lalistat and orlistat in rat HSCs, both on protein and mRNA levels (Figs. 3*A* and 9). The potency of the LAL inhibitors of the class of pyrazole-methanone compounds, E4, F2, and H4, to inhibit α-SMA expression correlated with their potency to inhibit neutral lipid degradation (*cf.* Fig. 1*D* and Fig. 9). In mouse HSCs lalistat, but not orlistat, inhibited HSC activation (Fig. 9). Orlistat was also less effective in mouse HSCs compared with lalistat and compared with its effect in rat HSCs in increasing the levels of TAGs, CEs, and REs (results not shown).

It has been reported that TAG degradation is required for the generation of FAs for energy during HSC activation in mouse stellate cell line JS1 (14). We, therefore, tested whether FAs derived from TAGs are required for the energy demand of rat HSCs under our culture conditions by treating the cells with etomoxir, an inhibitor of FA oxidation. However, we did not observe an effect of this inhibitor on rat HSC activation (Fig. 9), although the effectiveness of the drug was confirmed by the observation of a 2-fold increase in TAG levels in the presence of this FA oxidation-inhibitor (results not shown). Thus, we consider it more likely that hydrolysis of a specific lalistat-sensitive LD pool is involved in HSC activation for other reasons.

Discussion

We show here that lalistat, a specific inhibitor of the Lipa gene product LAL, affects the levels of three subtypes of neutral lipids, *i.e.* CEs, TAGs, and REs, in rat and mouse HSCs. The lalistat-induced increase in CEs is in line with the established function of LAL in degrading CEs from lipoproteins in the lysosome (18, 19). As expected, the increase was much lower in medium depleted of lipoproteins. The residual increase in the absence of exogenous lipoproteins may be caused by inhibiting the degradation of CEs delivered to the lysosome by the autophagy pathway, similarly to that described in macrophages (16, 30). Orlistat was less potent in comparison to lalistat in inhibiting the breakdown of CEs, indicating that it inhibited LAL to a lesser degree in HSCs at the concentration used.

LD pools

The comparison between the effects of the inhibitors lalistat and orlistat on TAG levels clearly indicated the existence of different pools of TAGs. Orlistat was more potent at inhibiting the degradation of newly synthesized TAGs, as judged from its large inhibitory effect on the breakdown of labeled TAGs. In contrast, lalistat was more potent in inhibiting the preexisting lipid pool as it did not inhibit the degradation of newly labeled TAGs but prevented the breakdown of existing TAGs when new TAG synthesis was blocked. We previously showed additional evidence for metabolically different TAG pools in HSCs from studies with ATGL$^{-/-}$ mice and the DGAT1 inhibitor T863 (9). We reported that the TAG lipase ATGL specifically targets newly synthesized PUFA-enriched TAGs, made preferentially by DGAT1 in combination with ACSL4. These newly formed TAGs are likely to form new LDs. By use of lalistat, we now have unmasked two pools of LDs by live cell-imaging of rat HSCs: one pool of LD-containing retinoids located predominately round the nucleus and a pool present in the periphery of the HSCs that did not contain REs. The combined breakdown of LDs in one place and re-synthesis in another would explain our previous observations in activated rat HSCs, *i.e.* that LDs reduce in size but increase in number and are localized in cellular extensions (4). Considering that in activated rat HSCs all LDs have a similar lipid spectrum containing a low amount of REs (4), we have to assume that REs are incorporated in the new LDs. Indeed, from D4-palmitate labeling studies and RE species

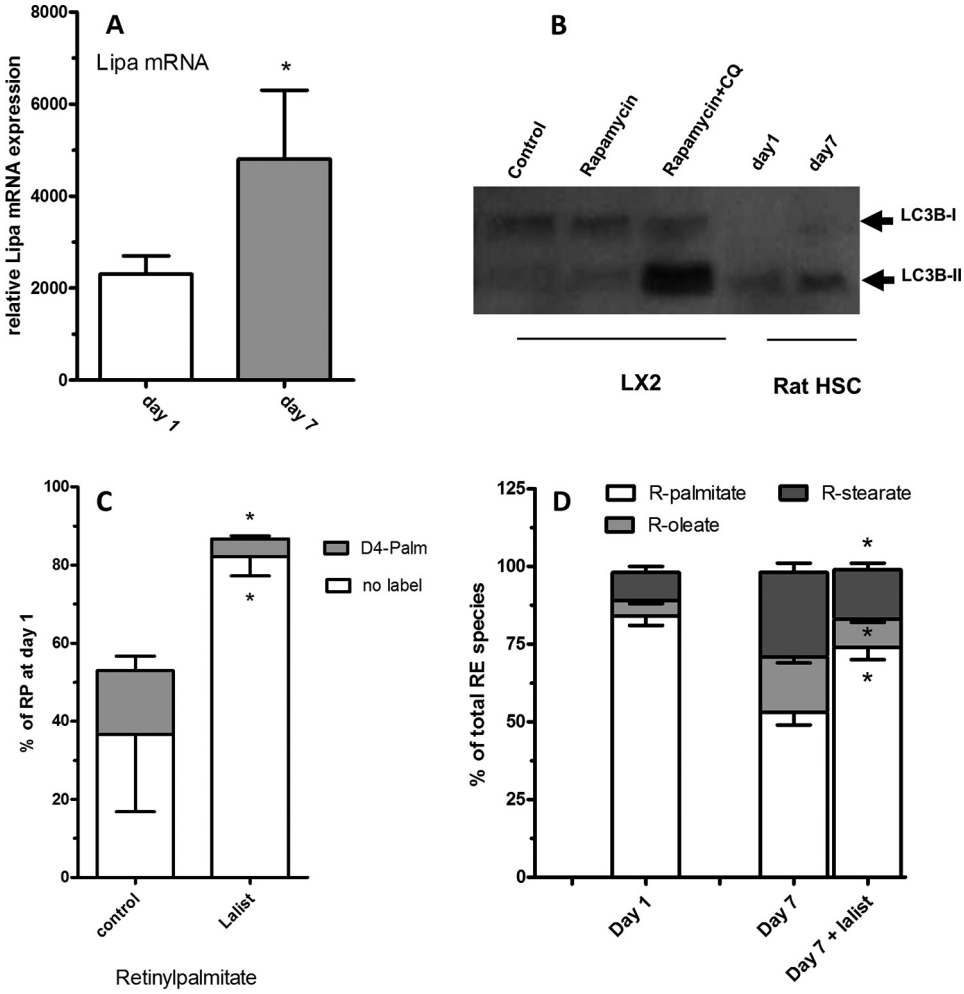

Figure 8. Expression of Lipa, activation of autophagy, and re-esterification of retinol in rat HSCs. *A*, relative mRNA expression of lysosomal acidic lipase LAL/Lipa in quiescent (*day 1*; *white bar*) and activated (*day 7*; *gray bar*) rat HSCs was determined by qPCR. *B*, immunoblot probed with LC3B antibody of total proteins (10 μg) of quiescent (*day 1*) and activated (*day 7*) rat HSCs and the human stellate cell line LX2 incubated for 4 h with vehicle (*control*), the autophagy inducer rapamycin (200 nM), or rapamycin in the presence of 20 μM chloroquine (*CQ*) to prevent breakdown of LC3B in the lysosome. LC3B-I is the non-activated form, and LC3B-II is the activated form containing the lipid phosphatidylethanolamine. Shown is a representative blot from three experiments. *C* and *D*, primary rat HSCs were either harvested at day 1 or incubated in medium with 10% FBS and 25 μM D4-palmitate-containing vehicle (DMSO; control) or with 100 μM lalistat (*Lalist*) for 3 days (day 1 to day 4; *C*) or incubated with medium with 10% FBS containing vehicle (DMSO; control) or with 100 μM lalistat (*Lalist*) for 6 days (day 1 to day 7; *D*). D4-labeled and non-labeled REs were quantitated by MRM. D4-labeled retinyl palmitate (*D4-Palm*) and non-labeled RP were expressed relative to the total RP levels at day 1 (*C*), or specific RE species were expressed as a percentage of total REs (*D*). Data are the means ± S.D. of three experiments performed in duplicate. *, $p < 0.05$ paired *t* test *versus* day 1 (*A*) or *versus* control (*C* and *D*).

distribution we have now evidence that REs, like TAGs, are partly re-synthesized during activation (8).

The lipase inhibitors orlistat and lalistat also caused a different effect on the morphology of the LDs. Lalistat increased the number but not the size of the LDs, whereas orlistat and Atglstatin (9) also increased the size of the LDs. This suggests that inhibition of lipase activity on the new LDs allow them to grow beyond a certain limit maintained under normal conditions by the consorted action of the TAG synthesizing enzyme (presumably DGAT1) and the TAG degrading activity (presumably ATGL). In contrast, lalistat-mediated accumulation of LDs reveals that the autophagy pathway engulfs lipid fragments around 0.8 μm, roughly similar to the size of the newly formed LDs (Fig. 3). This would be compatible with the reported sizes of autophagosomes ranging between 0.50 and 1.5 μm (31, 32) and with the observation in rat HSCs analyzed by EM that the subpopulation of LDs that was surrounded by lysosomes was smaller than the cytosolic LDs (33). A model of lipid metabolism and the formation of the different LD pools in HSCs is depicted in supplemental Fig. S3.

Lipa and retinyl ester hydrolysis

Besides inhibiting the degradation of CEs and TAGs, lalistat proved to be a potent inhibitor of RE degradation. As we observed REs in the acidic compartment after treatment with lalistat, a lysosomal lipase is involved in the breakdown of REs in activated HSCs. The most likely REH is Lipa/LAL as we found that it has clear REH activity *in vitro*. These findings are in line with similar results described recently by Grumet *et al.* (34). The REs are most likely delivered to the lysosomes by the autophagy pathway known to be active in activated HSCs (13–15) (Fig. 8). Unfortunately, we could not assess the contribution of the autophagy pathway in the degradation of REs by using autophagy inhibitors, as these inhibitors affected the viability of the primary rat and mouse HSCs under our conditions.

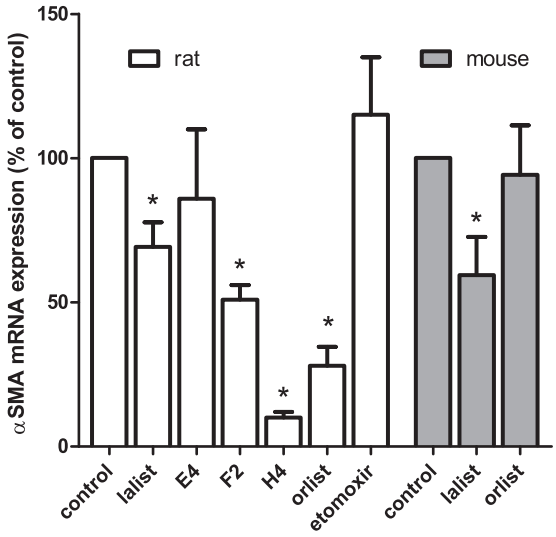

Figure 9. Effect of alterations in neutral lipid metabolism on activation of rat and mouse HSCs. Relative gene expression of α-SMA (HSC activation marker) was measured by qPCR. HSCs isolated from rats or mice were incubated from day 1 to day 7 with vehicle (DMSO; *control*), 100 μM lalistat (*lalist*), 40 μM orlistat (*orlist*), 10 μM pyrazole-methanone compounds E4, F2, or H4, or 50 μM etomoxir. Relative mRNA levels of α-SMA were expressed relative to the levels in the control-treated cells ($n = 5$ or $n = 3$ in the case of E4, F2, and H4). Data are the means ± S.D. *, $p < 0.05$ *t* test *versus* control.

An additional non-Lipa/non-autophagy degradation pathway for REs likely exists in mouse HSCs. RE levels in mouse HSC drop by ~90% from day 1 to day 7 (9), implying that only 10% is left at day 7. The 2.5-fold increase seen in the presence of lalistat indicates that still 75% of the RE pool has disappeared from the mouse HSCs in the presence of the LAL inhibitor. For comparison, rat HSCs at day 7 still has 30–20% of the RE content of day 1 in the absence of lalistat (4) and retain most of their REs in the presence of this inhibitor. Preliminary microarray data revealed that the expression of Lipa in mouse HSCs was almost halved at day 7 compared with day 1, whereas we found a 2-fold up-regulation in rat HSCs during activation (Fig. 8). A number of neutral carboxyl esterases was found to have REH activity, including ES4, ES10, and ES22 (35). The patatin-like phospholipase domain-containing 3 (PNPLA3) protein was also shown to have retinyl-palmitate lipase activity in human hepatic stellate cells (36). However, the relative contribution of any of these enzymes in RE degradation in HSCs upon activation is unknown.

Despite the capacity of LAL to degrade REs, no accumulation of REs was found in livers from LAL-deficient mice as was observed for CEs. In contrast, young (7-week-old mice) $Lipa^{-/-}$ mice had even lower liver levels of REs compared with WT mice, and livers of older mice (20 weeks) were almost devoid of RE stores. Retinoid storage in the liver is thought to be composed of multiple stages. Dietary retinoids are initially packaged as REs in chylomicrons by intestinal cells. The chylomicron remnants are taken up by hepatocytes and degraded in a supposedly non-lysosomal compartment (37). Subsequently, retinol is transferred from the hepatocytes to HSCs, where it is esterified by LRAT and stored in LDs (35). The lower storage of REs in the liver of the LAL-deficient mice may, therefore, point at a role of LAL in RE degradation in other cell types besides activated HSCs. The lower levels of REs in the livers of the LAL-deficient mice were also recently observed by Grumet *et al.* (34). They found a different retinoid handling in the intestine as a contributing factor to the lower RE levels in the liver. Furthermore, the here-observed role of LAL in degrading REs in activated HSCs, which have an active autophagy pathway, may be less prominent in quiescent HSCs in a healthy liver.

LRAT expression, a marker for quiescent HSCs (27), was not affected in the young $Lipa^{-/-}$ mice but was lost in the older mice, concomitant with a further loss in REs. This suggests that the REs in the young mice are presumably stored predominantly in HSCs, as in the older mice REs stores were probably decreased due to a loss of quiescent HSCs. The HSCs were not yet fully activated in the 20-week-old $Lipa^{-/-}$ mice, as we found no up-regulation of the HSC activation marker α-SMA. In earlier studies on the $Lipa^{-/-}$ mice, it was described that in young mice (1.5 months) lipid (CE/TAG) was predominantly accumulated in hepatocytes but that in older mice (5–8 months) macrophages became the major lipid-storing cells (38). This suggests that the influx of macrophages might be the cause of the disappearance of quiescent HSCs in the 20-week-old $Lipa^{-/-}$ mice. The absence of quiescent HSCs is probably followed by a fibrotic stage, as in older (24 weeks) Lipa-deficient mice clear liver fibrosis was detected (39). Likewise humans with mutations in Lipa are known to develop liver fibrosis (19).

Lipa and HSC function

The effect of lalistat, the pyrazole-methanone compounds E4, F2, and H4 and orlistat on lipid levels in rat and mouse HSCs generally correlated with their effect on HSC activation. Lalistat increased all classes of neutral lipids in both rat and mouse HSCs and attenuated activation in rat and mouse HSCs to a similar, albeit relatively low degree (30–40%, Fig. 9). Orlistat was more potent in rat HSCs as compared with mouse cells both in increasing neutral lipid levels and preventing activation. The inhibitory effect of lalistat and orlistat on rat HSC activation was comparable with the effect of another lipase inhibitor, Atglistatin (9). In comparison with lalistat, Atglistatin is more potent in inhibiting TAG breakdown but less potent in preventing RE and CE degradation. Although we cannot exclude the possibility that these drugs affect HSCs activation by other, non-lipid related pathways, their effects on HSC activation correlated with their effect on of neutral lipid breakdown. Therefore, it seems that HSCs require an available TAG/RE pool for optimal functioning. This pool may act as a buffer for FAs required for energy (14) or synthesis of membranes or bioactive lipids, like prostanoids. In rat HSCs we could not find evidence for a requirement for FA as a source of energy, as the β-oxidation inhibitor etomoxir did not affect activation. Another possibility would be that the neutral lipids by their physical presence in the cytosol, interfere with the differentiation processes needed for activation, like ER and Golgi expansion. This would also explain that mouse HSCs containing almost no LDs by a lack of LRAT show a normal activation response to liver injury (27).

Experimental procedures

Reagents

Lalistat (lalistat-2; 3,4-disubstituted thiadiazole carbamate, compound 12 from Rosenbaum *et al.* (21), was a gift from Paul Helquist (University of Notre Dame). The pyrazole-methanone compounds E4, F2, and H4 were described in VanderVen *et al.* (23). D4-palmitate and 3-methyladenine were purchased from Cayman Chemical (Ann Arbor, MI). D7-cholesteryl palmitate was from Avanti polar lipids. Dulbecco's modified Eagle's medium (DMEM), fetal bovine serum (FBS), and penicillin/streptomycin were obtained from Gibco. Bovine serum albumin (BSA) fraction V was obtained from PAA (Pasching, Austria). T863, chloroquine diphosphate salt, bafilomycin A, L-α-phosphatidylcholine, retinyl palmitate (RP), collagenase (*Clostridium histolyticum* Type I), and basic chemicals were obtained from Sigma. The mouse monoclonal antibody against α-SMA was from Thermo Scientific (Waltham, MA), and the rabbit polyclonal antibody against LC3B was from Novus Biologicals (Littleton, CO; catalog number NB600-1384). Lipid droplet staining dye LD540 was kindly donated by Dr. C. Thiele, University of Bonn, Bonn, Germany. Hoechst 33342 and HCS LipidTOX^{TM} Red neutral lipid stain were obtained from Molecular Probes (Eugene, OR), and paraformaldehyde (PF) (8%) was obtained from Electron Microscopy Sciences (Hatfield, PA). FluorSave was purchased from Calbiochem, and all HPLC-MS solvents were from Biosolve (Valkenswaard, The Netherlands) with exception of chloroform (Carl Roth, Karlsruhe, Germany) and were of HPLC grade. Silica-G (0.063–0.200 mm) was purchased from Merck. Delipidated FBS was made from FBS by extraction with diisopropyl ether and *n*-butyl alcohol (FBS/diisopropyl ether/*n*-butyl alcohol, 10/8/4 v/v/v) followed by extensive dialysis against phosphate-buffered saline (PBS) at 4 °C.

Animals

We used adult male Wistar rats (300–400 g) and 10–12-week-old male and female C57BL/6J mice for HSC isolation. Lipa$^{-/-}$ mice were generated as described (18). Procedures of rat and mouse care and handling were in accordance with governmental and international guidelines on animal experimentation and were approved by the Animal Experimentation Committee (Dierexperimentencommissie; DEC) of Utrecht University (DEC numbers 2010.III.09.110, 2012. III.10.100, and 2013.III.09.065).

HSC isolation and in vitro primary cell culture

Stellate cells were isolated from livers of rats and mice by collagenase digestion followed by differential centrifugation (40). After isolation, HSCs were plated in 24-, 12-, or 6-well plates at a density of 2×10^4, 5×10^4, or 1×10^5 cells/well, respectively. Cells were cultured in DMEM supplemented with 10% FBS, 100 units/ml penicillin, 100 μg/ml streptomycin, and 4 μl/ml Fungizone in a humidified 5% CO_2 incubator at 37 °C and were protected from light by covering with aluminum foil. Medium was changed every 3 days. Cell viability and cytotoxicity was assayed with the Cell Counting Kit-8 according to the instructions provided by the manufacturer (Dojindo Molecular Technologies, Inc., Rockville, MD).

RNA isolation, cDNA synthesis, and quantitative PCR

Total RNA was isolated using the RNeasy Mini Kit (Qiagen, Venlo, The Netherlands) including the optional on-column DNase digestion (Qiagen RNase-free DNase kit). RNA was dissolved in 30 μl of RNase free water and quantified by a Nanodrop ND-1000 (Isogen Life Science, IJsselstein, The Netherlands). An iScript cDNA Synthesis Kit (Bio-Rad) was used to synthesize cDNA. Primer design and quantitative PCR (qPCR) conditions were as described previously (41). Briefly, qPCR reactions were performed in duplicate using a Bio-Rad detection system. Amplifications were carried out in a volume of 25 μl containing 12.5 μl of 2×SYBR Green supermix (Bio-Rad), 1 μl of forward and reverse primer, and 1 μl of cDNA. Cycling conditions were as follows: initial denaturation at 95 °C for 3 min followed by 45 cycles of denaturation (95 °C for 10 s), annealing (temperature as described in supplemental Table S1 or Tuohetahuntila *et al.* (9) for 30 s), and elongation (72 °C for 30 s). A melting curve analysis was performed for every reaction. To determine relative expression of a gene, a 4-fold dilution series from a pool of all samples were used. IQ5 Real-Time PCR detection system software (Bio-Rad) was used for data analysis. Expression levels were normalized by using the average relative amount of reference genes. Reference genes used for normalization were based on their stable expression in stellate cells, namely, tyrosine 3-monooxygenase/tryptophan 5-monooxygenase activation protein, zeta (*Ywhaz*), hypoxanthine phosphoribosyltransferase (*Hprt*), and hydroxylmethylbilane synthase (*Hmbs*). Primers of reference genes are as described Tuohetahuntila *et al.* (9), and primers of target genes are listed in supplemental Table S1.

Immunofluorescence

Freshly isolated HSCs grown on glass coverslips in 24-well plates at 37 °C for 7 days were fixed in 4% (v/v) PF at room temperature for 30 min and stored in 1% (v/v) PF at 4 °C for a maximum of 1 week. Before staining, HSCs were washed twice in PBS, permeabilized by saponin (0.1% (w/v); Riedel-de Haën, Seelze, Germany), and blocked with 2% BSA in PBS for 1 h at room temperature. After blocking, cells were incubated for 1 h with the primary antibody against α-SMA (50–75 μg/ml), washed again, and incubated for 1 h with a fluorescently labeled secondary antibody (15 μg/ml) supplemented with Hoechst (4 μg/ml) for nuclear counterstaining and lipid droplet dye LD540 (0.05 μg/ml). Thereafter, coverslips were mounted with FluorSave on microscopic slides, and image acquisition was performed at the Center of Cellular Imaging, Faculty of Veterinary Medicine, Utrecht University on a Leica TCS SPE-II confocal microscope. To quantify lipid droplet size and numbers per cell, confocal images of LD540 (lipid droplets) and Hoechst33342 (nuclei) were analyzed with CellProfiler v2.1.1. Recognized lipid droplets and nuclei were overlaid on the original image to confirm the identity. The error rate was $<$5% for lipid droplets and $<$2% for nuclei.

Live cell imaging

For live cell imaging, cells (20-μl cell suspensions, $\sim 2 \times 10^5$ cells/ml) were plated on an 8-well glass-bottom slide from Ibidi (Planegg/Martinsried, Germany). Cells were cultured under similar conditions as described above in the presence or absence of lalistat for 3 days. At the 4th day after isolation, media were changed with fresh media 2 h before imaging. Just before imaging lysosomes in combination with LDs, 100 μl of Lysotracker Red DND99 (Life Technologies, final concentration of 75 nM) and Bodipy 493/503 (Molecular Probes, final concentration of 200 nM) were added for 30 min in the incubator. For detection of autophagy the Cyto-ID® Autophagy Detection Kit was used following the protocol supplied by the manufacturer (Enzo Life Sciences, Inc. Farmingdale, NY) with co-staining of the LDs with HCS LipidTOX™ Red neutral lipid. Images of the samples were recorded using a NIKON A1R confocal microscope equipped with a humidified imaging chamber set to 5% CO_2 and 37 °C (TOKAI hit, Japan) at the Center for Cell Imaging (CCI), Faculty of Veterinary Medicine, Utrecht University.

REH and cholesteryl esterase activity assay

REH was assayed essential as described (25). In short, an aliquot of homogenized mouse liver (400 μg of protein), homogenized rat hepatocytes (400 μg of protein), or rat HSCs (16 μg of protein) were incubated in 100 μl of sodium citrate buffer (60 mM; pH 4.1) or HEPES buffer (60 mM; pH 7) at 37 °C in a shaking water bath for 45 min in the presence of 1.9 mM RP and/or 1.5 mM D7-cholesteryl palmitate (D7-CE) incorporated into liposomes. Liposomes were made by dissolving 20 mg of L-α-phosphatidylcholine and 0.5 mg of RP and/or 0.5 mg of D7-CE in chloroform. After solvent evaporation, the lipids were suspended in 1 ml of 50 mM NaCl and 10 mM Tris, pH 7.4, by sonication and centrifuged at 17,300 $\times$ *g* for 10 min to sediment large vesicles. The reaction was stopped by the addition of 100 μl of ethanol, and lipids were determined by HPLC-MS using multiple reaction monitoring (MRM) (8).

Analysis of neutral lipids by HPLC-MS

Lipids were extracted from a total cell homogenate of HSCs grown in a 12-well plate by the method of Bligh and Dyer (42) after the addition of 200 pmol of tripentadecanoylglycerol as the internal standard. Extracted lipids were separated in a neutral and phospholipid fraction and analyzed on HPLC-MS as described (9). In short, the neutral lipid fraction was reconstituted in methanol/chloroform (1/1, v/v) and separated on a Kinetex/HALO C8-e column by a gradient of methanol/H_2O (5/5, v/v) to methanol/isopropyl alcohol (8/2, v/v). Mass spectrometry of neutral lipids (TAGs, CEs, REs, and cholesterol) was performed using Atmospheric Pressure Chemical Ionization (APCI) interface (AB Sciex Instruments, Toronto, ON, Canada) on a Biosystems API-2000 Q-trap mass spectrometer. The system was controlled by Analyst version 1.4.2 software (MDS Sciex, Concord, ON, Canada) and operated in positive-ion mode. TAG fragments with two non-, single-, and double-labeled palmitoyl chains (16:0,16:0,*x*) were quantitated by counting ions with *m*/*z* of 551, 555, and 559, respectively. Typical TAG species quantitated were: non PUFA, 52:3 (*m*/*z* 859) and 54:3 (*m*/*z* 885); 1×PUFA, 56:5 (*m*/*z* 909) and 58:6 (*m*/*z* 935); 2×PUFA 60:9 (*m*/*z* 957) and 62:11 (*m*/*z* 981). For the quantification of the various (deuterated) RE and CE species, we used MRM in positive-ion mode by monitoring molecule specific transitions as described (8). Specific transitions analyzed are summarized in supplemental Table S2. The quantitated lipids were normalized to the amount of cholesterol or protein in the same sample. Cholesterol was found to be a good marker for both recovery and cellular material, as the cholesterol/protein ratio was found to be constant during HSC culture.

Statistical analysis

Each experiment was performed in duplicate and repeated at least three times. Comparisons of a variable between two groups were made with unpaired or paired Student's *t* test depending on whether the data were normalized to a control before analysis. Differences were considered statistically significant for p values <0.05.

Author contributions—M. T. designed, performed, and analyzed the experiments and contributed in the writing of the paper. M. R. M. contributed to the performance and analysis of the imaging experiments and the retinoid determinations. B. S. helped with designing and performing of the qPCR experiments. J. F. B. helped with design, performance, and analysis of the lipidomic experiments. R. W. contributed to the design, performance, and analysis of the imaging experiments. M. H. contributed to the design and performance of the HSC isolation and culture and interpretation of the lipidomic data. C. Y. and H. D. contributed to the design and performance of the experiments with the Lipa deficient livers. B. C. V. contributed to the design and performance of the experiments with the pyrazolemethanone class LAL-inhibitors. A. B. V. and J. B. H. conceived and coordinated the study and wrote the paper. All authors analyzed the results and approved the final version of the manuscript.

Acknowledgments—We acknowledge Jeroen Jansen for technical assistance with the lipid analysis. We also thank Paul Helquist (University of Notre Dame) for donating the lalistat2 compound. Real time quantitative PCR was performed and mouse reference gene primers were provided by the Department of Clinical Sciences of Companion Animals, Faculty of Veterinary Medicine, Utrecht University. Images were acquired at the Center of Cellular Imaging, Faculty of Veterinary Medicine, Utrecht University on a Leica TCS SPE-II confocal microscope, and we thank Esther van't Veld for assistance.

References

1. Blaner, W. S., O'Byrne, S. M., Wongsiriroj, N., Kluwe, J., D'Ambrosio, D. M., Jiang, H., Schwabe, R. F., Hillman, E. M., Piantedosi, R., and Libien, J. (2009) Hepatic stellate cell lipid droplets: a specialized lipid droplet for retinoid storage. *Biochim. Biophys. Acta* **1791,** 467–473
2. Friedman, S. L. (2008) Hepatic stellate cells: protean, multifunctional, and enigmatic cells of the liver. *Physiol. Rev.* **88,** 125–172
3. Pellicoro, A., Ramachandran, P., Iredale, J. P., and Fallowfield, J. A. (2014) Liver fibrosis and repair: immune regulation of wound healing in a solid organ. *Nat. Rev. Immunol.* **14,** 181–194
4. Testerink, N., Ajat, M., Houweling, M., Brouwers, J. F., Pully, V. V., van Manen, H. J., Otto, C., Helms, J. B., and Vaandrager, A. B. (2012) Replacement of retinyl esters by polyunsaturated triacylglycerol species in lipid droplets of hepatic stellate cells during activation. *PLoS ONE* **7,** e34945

5. Tuohetahuntila, M., Spee, B., Kruitwagen, H. S., Wubbolts, R., Brouwers, J. F., van de Lest, C. H., Molenaar, M. R., Houweling, M., Helms, J. B., and Vaandrager, A. B. (2015) Role of long-chain acyl-CoA synthetase 4 in formation of polyunsaturated lipid species in hepatic stellate cells. *Biochim. Biophys. Acta* **1851,** 220–230
6. Wilfling, F., Haas, J. T., Walther, T. C., and Farese R. V., Jr. (2014) Lipid droplet biogenesis. *Curr. Opin. Cell Biol.* **29,** 39–45
7. Long, A. P., Manneschmidt, A. K., VerBrugge, B., Dortch, M. R., Minkin, S. C., Prater, K. E., Biggerstaff, J. P., Dunlap, J. R., and Dalhaimer, P. (2012) Lipid droplet de novo formation and fission are linked to the cell cycle in fission yeast. *Traffic* **13,** 705–714
8. Ajat, M., Molenaar, M., Brouwers, J. F., Vaandrager, A. B., Houweling, M., and Helms, J. B. (2017) Hepatic stellate cells retain the capacity to synthesize retinyl esters and to store neutral lipids in small lipid droplets in the absence of LRAT. *Biochim. Biophys. Acta* **1862,** 176–187
9. Tuohetahuntila, M., Molenaar, M. R., Spee, B., Brouwers, J. F., Houweling, M., Vaandrager, A. B., and Helms, J. B. (2016) ATGL and DGAT1 are involved in the turnover of newly synthesized triacylglycerols in hepatic stellate cells. *J. Lipid Res.* **57,** 1162–1174
10. Zechner, R., Kienesberger, P. C., Haemmerle, G., Zimmermann, R., and Lass, A. (2009) Adipose triglyceride lipase and the lipolytic catabolism of cellular fat stores. *J. Lipid Res.* **50,** 3–21
11. Schweiger, M., Lass, A., Zimmermann, R., Eichmann, T. O., and Zechner, R. (2009) Neutral lipid storage disease: genetic disorders caused by mutations in adipose triglyceride lipase/PNPLA2 or CGI-58/ABHD5. *Am. J. Physiol. Endocrinol. Metab.* **297,** E289–E296
12. Mello, T., Nakatsuka, A., Fears, S., Davis, W., Tsukamoto, H., Bosron, W. F., and Sanghani, S. P. (2008) Expression of carboxylesterase and lipase genes in rat liver cell types. *Biochem. Biophys. Res. Commun.* **374,** 460–464
13. Thoen, L. F., Guimarães, E. L., Dollé, L., Mannaerts, I., Najimi, M., Sokal, E., and van Grunsven, L. A. (2011) A role for autophagy during hepatic stellate cell activation. *J. Hepatol.* **55,** 1353–1360
14. Hernández-Gea, V., Ghiassi-Nejad, Z., Rozenfeld, R., Gordon, R., Fiel, M. I., Yue, Z., Czaja, M. J., and Friedman, S. L. (2012) Autophagy releases lipid that promotes fibrogenesis by activated hepatic stellate cells in mice and in human tissues. *Gastroenterology* **142,** 938–946
15. Zhang, Z., Zhao, S., Yao, Z., Wang, L., Shao, J., Chen, A., Zhang, F., and Zheng, S. (2017) Autophagy regulates turnover of lipid droplets via ROS-dependent Rab25 activation in hepatic stellate cell. *Redox Biol.* **11,** 322–334
16. Ouimet, M., Franklin, V., Mak, E., Liao, X., Tabas, I., and Marcel, Y. L. (2011) Autophagy regulates cholesterol efflux from macrophage foam cells via lysosomal acid lipase. *Cell. Metab.* **13,** 655–667
17. Brown, M. S., and Goldstein, J. L. (1986) A receptor-mediated pathway for cholesterol homeostasis. *Science* **232,** 34–47
18. Du, H., Duanmu, M., Witte, D., and Grabowski, G. A. (1998) Targeted disruption of the mouse lysosomal acid lipase gene: long-term survival with massive cholesteryl ester and triglyceride storage. *Hum. Mol. Genet.* **7,** 1347–1354
19. Anderson, R. A., Bryson, G. M., and Parks, J. S. (1999) Lysosomal acid lipase mutations that determine phenotype in Wolman and cholesterol ester storage disease. *Mol. Genet. Metab.* **68,** 333–345
20. Rosenbaum, A. I., Rujoi, M., Huang, A. Y., Du, H., Grabowski, G. A., and Maxfield, F. R. (2009) Chemical screen to reduce sterol accumulation in Niemann-Pick C disease cells identifies novel lysosomal acid lipase inhibitors. *Biochim. Biophys. Acta* **1791,** 1155–1165
21. Rosenbaum, A. I., Cosner, C. C., Mariani, C. J., Maxfield, F. R., Wiest, O., and Helquist, P. (2010) Thiadiazole carbamates: potent inhibitors of lysosomal acid lipase and potential Niemann-Pick type C disease therapeutics. *J. Med. Chem.* **53,** 5281–5289
22. Hamilton, J., Jones, I., Srivastava, R., and Galloway, P. (2012) A new method for the measurement of lysosomal acid lipase in dried blood spots using the inhibitor Lalistat 2. *Clin. Chim. Acta* **413,** 1207–1210
23. VanderVen, B. C., Hermetter, A., Huang, A., Maxfield, F. R., Russell, D. G., and Yates, R. M. (2010) Development of a novel, cell-based chemical screen to identify inhibitors of intraphagosomal lipolysis in macrophages. *Cytometry A* **77,** 751–760
24. Borgström, B. (1988) Mode of action of tetrahydrolipstatin: a derivative of the naturally occurring lipase inhibitor lipstatin. *Biochim. Biophys. Acta* **962,** 308–316
25. Mercier, M., Forget, A., Grolier, P., and Azais-Braesco, V. (1994) Hydrolysis of retinyl esters in rat liver: description of a lysosomal activity. *Biochim. Biophys. Acta* **1212,** 176–182
26. Azaïs-Braesco, V., Dodeman, I., Delpal, S., Alexandre-Gouabau, M. C., Partier, A., Borel, P., and Grolier, P. (1995) Vitamin A contained in the lipid droplets of rat liver stellate cells is substrate for acid retinyl ester hydrolase. *Biochim. Biophys. Acta* **1259,** 271–276
27. Kluwe, J., Wongsiriroj, N., Troeger, J. S., Gwak, G. Y., Dapito, D. H., Pradere, J. P., Jiang, H., Siddiqi, M., Piantedosi, R., O'Byrne, S. M., Blaner, W. S., and Schwabe, R. F. (2011) Absence of hepatic stellate cell retinoid lipid droplets does not enhance hepatic fibrosis but decreases hepatic carcinogenesis. *Gut* **60,** 1260–1268
28. Kabeya, Y., Mizushima, N., Yamamoto, A., Oshitani-Okamoto, S., Ohsumi, Y., and Yoshimori, T. (2004) LC3, GABARAP and GATE16 localize to autophagosomal membrane depending on form-II formation. *J. Cell Sci.* **117,** 2805–2812
29. Xu, L., Hui, A. Y., Albanis, E., Arthur, M. J., O'Byrne, S. M., Blaner, W. S., Mukherjee, P., Friedman, S. L., and Eng, F. J. (2005) Human hepatic stellate cell lines, LX-1 and LX-2: new tools for analysis of hepatic fibrosis. *Gut* **54,** 142–151
30. Robinet, P., Ritchey, B., and Smith, J. D. (2013) Physiological difference in autophagic flux in macrophages from 2 mouse strains regulates cholesterol ester metabolism. *Arterioscler. Thromb. Vasc. Biol.* **33,** 903–910
31. Bains, M., Florez-McClure, M. L., and Heidenreich, K. A. (2009) Insulin-like growth factor-I prevents the accumulation of autophagic vesicles and cell death in Purkinje neurons by increasing the rate of autophagosome-to-lysosome fusion and degradation. *J. Biol. Chem.* **284,** 20398–20407
32. Mizushima, N., Ohsumi, Y., and Yoshimori, T. (2002) Autophagosome formation in mammalian cells. *Cell Struct. Funct.* **27,** 421–429
33. Yamamoto, K., and Ogawa, K. (1983) Fine structure and cytochemistry of lysosomes in the Ito cells of the rat liver. *Cell Tissue Res.* **233,** 45–57
34. Grumet, L., Eichmann, T. O., Taschler, U., Zierler, K. A., Leopold, C., Moustafa, T., Radovic, B., Romauch, M., Yan, C., Du, H., Haemmerle, G., Zechner, R., Fickert, P., Kratky, D., Zimmermann, R., and Lass, A. (2016) Lysosomal acid lipase hydrolyzes retinyl ester and affects retinoid turnover. *J. Biol. Chem.* **291,** 17977–17987
35. Schreiber, R., Taschler, U., Preiss-Landl, K., Wongsiriroj, N., Zimmermann, R., and Lass, A. (2012) Retinyl ester hydrolases and their roles in vitamin A homeostasis. *Biochim. Biophys. Acta* **1821,** 113–123
36. Pirazzi, C., Valenti, L., Motta, B. M., Pingitore, P., Hedfalk, K., Mancina, R. M., Burza, M. A., Indiveri, C., Ferro, Y., Montalcini, T., Maglio, C., Dongiovanni, P., Fargion, S., Rametta, R., Pujia, A., Andersson, L., *et al.* (2014) PNPLA3 has retinyl-palmitate lipase activity in human hepatic stellate cells. *Hum. Mol. Genet.* **23,** 4077–4085
37. Blomhoff, R., Eskild, W., Kindberg, G. M., Prydz, K., and Berg, T. (1985) Intracellular transport of endocytosed chylomicron [^{3}H]retinyl ester in rat liver parenchymal cells. Evidence for translocation of a [^{3}H]retinoid from endosomes to endoplasmic reticulum. *J. Biol. Chem.* **260,** 13566–13570
38. Du, H., Heur, M., Duanmu, M., Grabowski, G. A., Hui, D. Y., Witte, D. P., and Mishra, J. (2001) Lysosomal acid lipase-deficient mice: depletion of white and brown fat, severe hepatosplenomegaly, and shortened life span. *J. Lipid Res.* **42,** 489–500
39. Sun, Y., Xu, Y. H., Du, H., Quinn, B., Liou, B., Stanton, L., Inskeep, V., Ran, H., Jakubowitz, P., Grilliot, N., and Grabowski, G. A. (2014) Reversal of advanced disease in lysosomal acid lipase deficient mice: a model for lysosomal acid lipase deficiency disease. *Mol. Genet. Metab.* **112,** 229–241
40. Riccalton-Banks, L., Bhandari, R., Fry, J., and Shakesheff, K. M. (2003) A simple method for the simultaneous isolation of stellate cells and hepatocytes from rat liver tissue. *Mol. Cell. Biochem.* **248,** 97–102
41. van Steenbeek, F. G., Van den Bossche, L., Grinwis, G. C., Kummeling, A., van Gils, I. H., Koerkamp, M. J., van Leenen, D., Holstege, F. C., Penning, L. C., Rothuizen, J., Leegwater, P. A., and Spee, B. (2013) Aberrant gene expression in dogs with portosystemic shunts. *PLoS ONE* **8,** e57662
42. Bligh, E. G., and Dyer, W. J. (1959) A rapid method of total lipid extraction and purification. *Can. J. Biochem. Physiol.* **37,** 911–917